Quasiparticle interference and superconducting gap in $Ca_{2-x}Na_xCuO_2Cl_2$

T. HANAGURI[1,2]*, Y. KOHSAKA[3], J. C. DAVIS[3,4], C. LUPIEN[5], I. YAMADA[6], M. AZUMA[6], M. TAKANO[6], K. OHISHI[7], M. ONO[1,2] AND H. TAKAGI[1,2,8]

[1]Magnetic Materials Laboratory, RIKEN (The Institute of Physical and Chemical Research), Wako 351-0198, Japan
[2]CREST, Japan Science and Technology Agency, Kawaguchi 332-0012, Japan
[3]LASSP, Department of Physics, Cornell University, Ithaca, New York 14853, USA
[4]CMPMS Department, Brookhaven National Laboratory, Upton, New York 11973, USA
[5]Département de Physique, Université de Sherbrooke, Sherbrooke, QC J1K 2R1, Canada
[6]Institute for Chemical Research, Kyoto University, Uji 601-0011, Japan
[7]Advanced Science Research Center, Japan Atomic Energy Agency, Ibaraki 319-1195, Japan
[8]Department of Advanced Materials, University of Tokyo, Kashiwa 277-8561, Japan
*e-mail: hanaguri@riken.jp

Published online: 28 October 2007; doi:10.1038/nphys753

High-transition-temperature (high-T_c) superconductivity is ubiquitous in the cuprates containing CuO_2 planes, but each cuprate has its own character. The study of the material dependence of the *d*-wave superconducting gap (SG) should provide important insights into the mechanism of high-T_c superconductivity. However, because of the 'pseudogap' phenomenon, it is often unclear whether the energy gaps observed by spectroscopic techniques really represent the SG. Here, we use scanning tunnelling spectroscopy to image nearly optimally doped $Ca_{2-x}Na_xCuO_2Cl_2$ (Na-CCOC) with $T_c = 25$–28 K. It enables us to observe the quasiparticle interference effect in this material, through which we obtain unambiguous information on the SG. Our analysis of quasiparticle interference in Na-CCOC reveals that the SG dispersion near the gap node is almost identical to that of $Bi_2Sr_2CaCu_2O_y$ (Bi2212) at the same doping level, despite the T_c of Bi2212 being three times higher than that of Na-CCOC. We also find that the SG in Na-CCOC is confined in narrower energy and momentum ranges than Bi2212, which explains—at least in part—the remarkable material dependence of T_c.

Recent progress in spectroscopic techniques has enabled the elucidation of various interesting aspects of the electronic states of high-T_c cuprates in real and momentum (**k**) spaces. Scanning tunnelling microscopy/spectroscopy (STM/STS) measurements have provided a wide variety of real-space information[1] including various types of electronic inhomogeneity[2–6] and the presence of energy non-dispersive 'checkerboard' (CB) modulations in the tunnelling-conductance map at location **r** and energy E, $g(\mathbf{r}, E) \equiv \mathrm{d}I/\mathrm{d}V(\mathbf{r}, E)$, where I is the tunnelling current and V is the bias voltage[7–10]. In **k** space, angle-resolved photoemission spectroscopy (ARPES) on the underdoped cuprates has revealed that coherent quasiparticle states exist only in the nodal region around $(\pi/2, \pi/2)$ (refs 11–14). Here, the ARPES spectra away from the node are very broad. As a result, the cylindrical Fermi surface (FS) centred around (π, π) is somehow 'truncated' around the first Brillouin zone face and ends up with a so-called 'Fermi arc' in **k** space[15]. The Fermi arc length increases with doping and the full FS is restored in the optimally/overdoped region[13,14].

It is very important to understand how superconductivity emerges from such a complicated situation. Because superconducting states are characterized by the SG, detailed information on the SG is indispensable. There is now consensus that the SG in cuprates has *d*-wave symmetry[16] and thus has nodes in **k** space. However, direct studies of the SG structure by spectroscopic techniques are still in a pioneering stage[1,11,14,16–19]. The reason is that, whereas energy gaps can be measured in cuprates, whether such gaps represent the true SG is often unclear because of the presence of the 'pseudogap'[20].

Here we choose spectroscopic imaging scanning tunnelling microscopy (SI-STM) as a tool to settle this issue. Of course, because of the electronic heterogeneity, the atomic spatial resolution of SI-STM is highly advantageous. Perhaps more importantly, by using Fourier transformations, we can now access the **k**-space electronic structure as well[10,21,22]. So far, numerous STM/STS studies have been carried out on Bi2212. Among them, the discovery of dispersive g modulations due to quasiparticle interference (QPI) in the *d*-wave superconducting state[10,21–31] and its use for simultaneous determination of the **k**-space region supporting the *d*-wave quasiparticles and the dispersion of the SG provided a completely new approach to studies of high-T_c superconductivity[10,21,22]. Conventional spectroscopies essentially give us only the density-of-states (DOS) spectrum and cannot distinguish the SG from the pseudogap. By contrast, when the observed QPI pattern is fully consistent within the 'octet' model[22], we can be certain that the data represent the true SG. (See the next section.) In spite of this great advantage, detailed information from QPI has been available only in Bi2212 (refs 10,21,22); the universal characterization of the cuprate SG using the QPI technique has not yet been achieved.

Here we report the QPI effect in nearly optimally doped Na-CCOC with $T_c = 25$–28 K. Although the CB g modulation dominates the STS data[9], the full octet model of QPI is confirmed

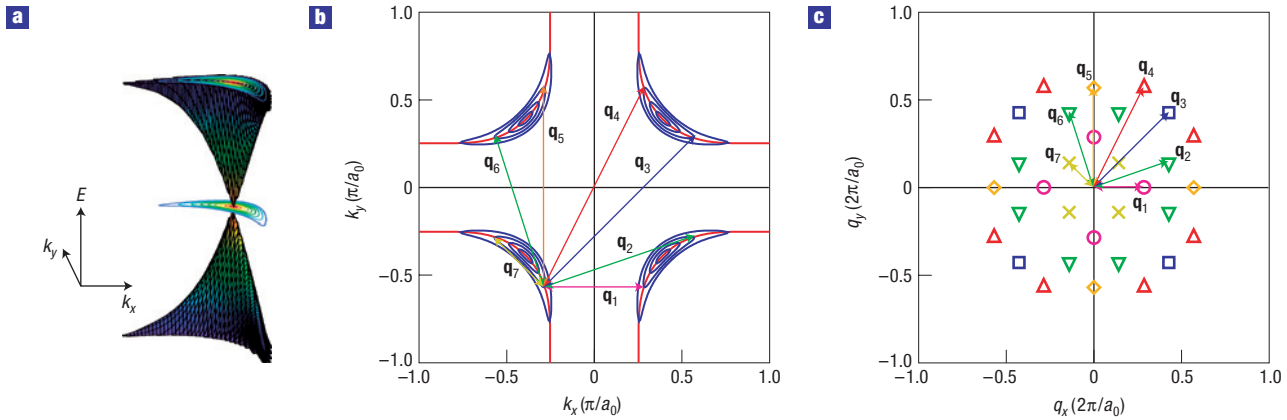

Figure 1 Schematic illustration of electronic states responsible for the interference effect of Bogoliubov quasiparticles in the superconducting state. a, A perspective view of the expected particle–hole-symmetric quasiparticle dispersion relation $\pm\sqrt{\varepsilon(\mathbf{k})^2+\Delta(\mathbf{k})^2}$ near one of the nodes showing a banana-shaped CCE. **b**, Four sets of CCEs (blue curves) in momentum space. The underlying FS is also shown by red curves. Note that the octet ends of 'bananas' track the FS. Because $\varepsilon(\mathbf{k})=0$ on the FS, the SG dispersion $\Delta(\mathbf{k})$ can be obtained by knowing the location of octet ends of 'bananas' in momentum space. Arrows denote expected scattering **q** vectors, which characterize the standing waves of quasiparticles at a specific energy. Each vector connects the octet ends of 'bananas' where the DOS is high. Here, a_0 denotes the Cu–Cu distance. **c**, The **q**-space representation of the QPI, which is directly associated with the Fourier transform of the conductance map $|g(\mathbf{q},E)|$. Symbols represent **q** vectors expected from the octet model[22]. The **q** vectors move with energy according to the FS shown in **b**. Thus the FS can be reconstructed and $\Delta(\mathbf{k})$ can be determined from energy-dependent **q** vectors.

by using the contrast of spatial-phase relations between CB g modulation and QPI. The SG is identified only on an 'arc' in **k** space near the gap node. No well-defined coherence peak is observed in the tunnelling spectrum and the antinodal region therefore remains incoherent. Thus, Na-CCOC shows the apparent coexistence of nodal superconductivity with the incoherent antinodal states as for the case of underdoped Bi2212 (ref. 10), indicating that these are universal features of high-T_c superconductivity. The SG dispersion of nearly optimally doped Na-CCOC is almost identical to that of optimally doped Bi2212 with $T_c=86$ K (ref. 22) but is confined in narrower energy and momentum ranges. From these observations we hypothesize that the energy scale which determines the T_c of optimally doped cuprates is not set by the superconducting gap dispersion alone but by the energy and momentum-space location where this gap terminates on the Fermi arc.

QPI AND THE OCTET MODEL

Originally, QPI was observed on conventional metal surfaces[32–34]. In the presence of elastic scattering, quantum interference of scattered electrons results in real-space electronic standing waves, characterized by wavevectors **q** connecting points on the contours of constant quasiparticle energy (CCEs) in **k** space. This standing wave can be detected using SI-STM by mapping $g(\mathbf{r},E)$, which reflects the local DOS. The wavevector **q** changes with E according to the electron-energy–dispersion relation. The Fourier amplitude of the conductance map, $|g(\mathbf{q},E)|$, enables us to determine characteristic **q** vectors at a given E. Therefore, the energy–dispersion relation can be obtained experimentally.

In the superconducting state, the Bardeen–Cooper–Schrieffer theory of superconductivity tells us that elementary excitations are not bare electrons or holes but coherent admixtures of particle and hole states known as Bogoliubov quasiparticles[35]. The excitation energy of a Bogoliubov quasiparticle $E(\mathbf{k})$ is given by $E(\mathbf{k})=\pm\sqrt{\varepsilon(\mathbf{k})^2+\Delta(\mathbf{k})^2}$, where $\varepsilon(\mathbf{k})$ is the normal-state band dispersion and $\Delta(\mathbf{k})$ is the SG. In the case of high-T_c cuprates, $\Delta(\mathbf{k})$ has d-wave symmetry and thus vanishes in the $(0,0)$–$(\pm\pi,\pm\pi)$ directions (nodes). Because Bogoliubov quasiparticles can be excited by either positive or negative energies and the Fermi velocity is much larger than the nodal gap slope, the excitation spectrum around the node is a particle–hole-symmetric thin Dirac cone with a banana-shaped CCE, as illustrated in Fig. 1a and b. QPI of Bogoliubov quasiparticles occurs in this situation[10,21–31]. The intensities of the standing waves with **q** vectors connecting the ends of 'bananas' should become large, because the DOS, which is inversely proportional to the slope of dispersion, becomes a maximum at the energy-dependent octet ends of 'bananas'. There are seven possible vectors $\mathbf{q}_i$ $(i=1$–$7)$ from one of the octet ends as shown in Fig. 1b. In total, 32 different **q** vectors (16 of them are independent) may be observed in $|g(\mathbf{q},E)|$ (Fig. 1c). If these numerous **q** vectors are observed in $|g(\mathbf{q},E)|$ and disperse with E according to the above-mentioned 'octet' model[22] in an internally consistent fashion, the presence of coherent Bogoliubov quasiparticles and the underling d-wave SG can be established without doubt. By analysing the E dependence of $\mathbf{q}_i$, we can deduce the locations of octet elements in **k** space, namely FS position, as well as the dispersion relation of the SG, $\Delta(\mathbf{k})$ (ref. 22). Although detailed calculations[23–31] are necessary to reproduce the observed intensity distribution in $|g(\mathbf{q},E)|$, the simple octet model on the basis of the DOS argument explains the observed **q** vectors in Bi2212 quite well and detailed information about the SG has been obtained[10,22].

SEARCH FOR QPI IN Na-CCOC

Bi2212 is the only material for which QPI has been detected so far. Only after identifying the SG in other cuprates by QPI can the universal features of the superconducting electronic state of cuprates be elucidated. Even more importantly, a clue to the cause of the strong variations of T_c from material to material may then be inferred. To carry out the search for QPI, we chose Na-CCOC (refs 36,37) as the next likeliest cuprate. Because Na-CCOC crystals cleave well, clean and flat surfaces necessary for STM/STS can be obtained easily. Previous STM/STS works on

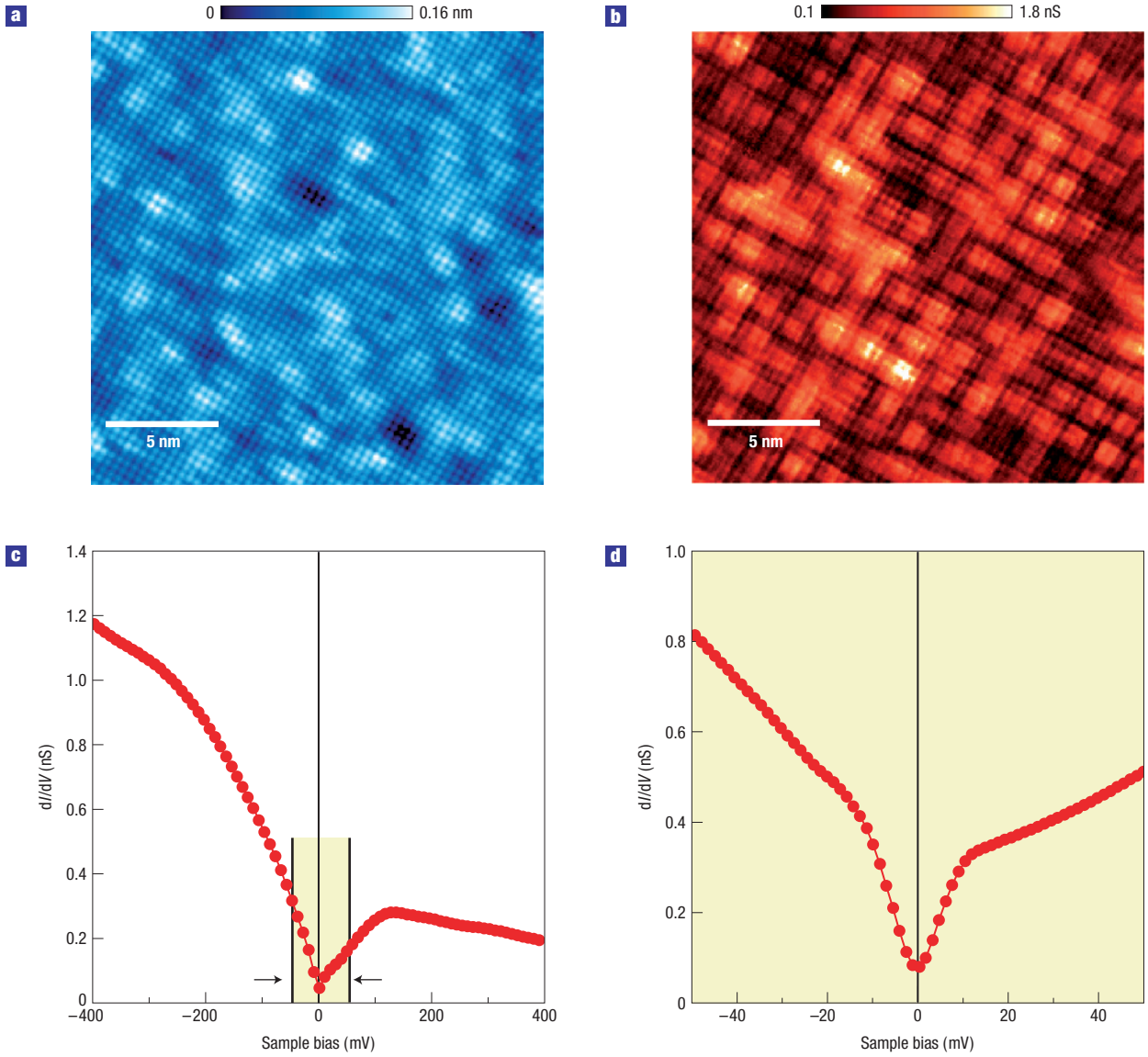

Figure 2 Spectroscopic features of nearly optimally doped Na-CCOC with $T_c \sim 25$ K ($x \sim 0.13$). **a**, Typical topographic STM image of Na-CCOC. The image was taken at a sample-bias voltage $V_s = +400$ mV and a tunnelling current $I_t = 100$ pA. All the spectroscopic images in this paper were taken simultaneously with similar atomic-resolution topographic images to maintain the atomic-resolution position registry. **b**, The conductance $g(\mathbf{r}, E)$ map at energy $E = +24$ meV in the same field of view. Apparent CB g modulation, which has been found in heavily underdoped Na-CCOC (ref. 9), is observed even in the nearly optimally doped sample. **c**, The spatially averaged conductance spectrum showing the V-shaped pseudogap below ~100 meV with particle–hole asymmetry at higher energies. (Set-up condition: $V_s = +400$ mV and $I_t = 100$ pA.) **d**, The spatially averaged spectrum in the low-energy region indicated by arrows in **c**, showing a pair of kinks in the spectrum inside the pseudogap. (Set-up condition: $V_s = +150$ mV and $I_t = 100$ pA.) The central interest of this paper is in the electronic state below and around this kink energy.

Na-CCOC have been carried out only in the heavily underdoped region, and revealed nanoscale electronic inhomogeneity[6] and CB g modulation[9]. However, no QPI signal was detected although the QPI signal may merely be too weak owing to the weakness of superconductivity in the heavily underdoped regime.

Recently, nearly optimally doped Na-CCOC single crystals ($T_c = 25$–28 K) have become available and we have searched for QPI in these samples (see the Methods section). It is important to notice that the crystal structure, the atomic species in the blocking layer between CuO_2 planes, the number of CuO_2 planes in the unit cell, and the T_c at optimal doping are all different between Na-CCOC and Bi2212. Because these materials are so completely disparate in the physics/chemistry of the blocking layers through which tunnelling occurs, common QPI phenomena must derive from the only common characteristic that is intrinsic to the electronic structure of the CuO_2 plane in which high-T_c superconductivity takes place.

Figure 2a shows a typical topographic image of the sample with $T_c \sim 25$ K. All the spectroscopic imaging measurements reported in this paper have been simultaneously carried out with similar atomic-resolution topographic images to maintain the position registry. The cleaved surfaces show a perfect square lattice with superimposed inhomogeneity, similar to the topographic images in the heavily underdoped samples[6,9]. Overall similarities

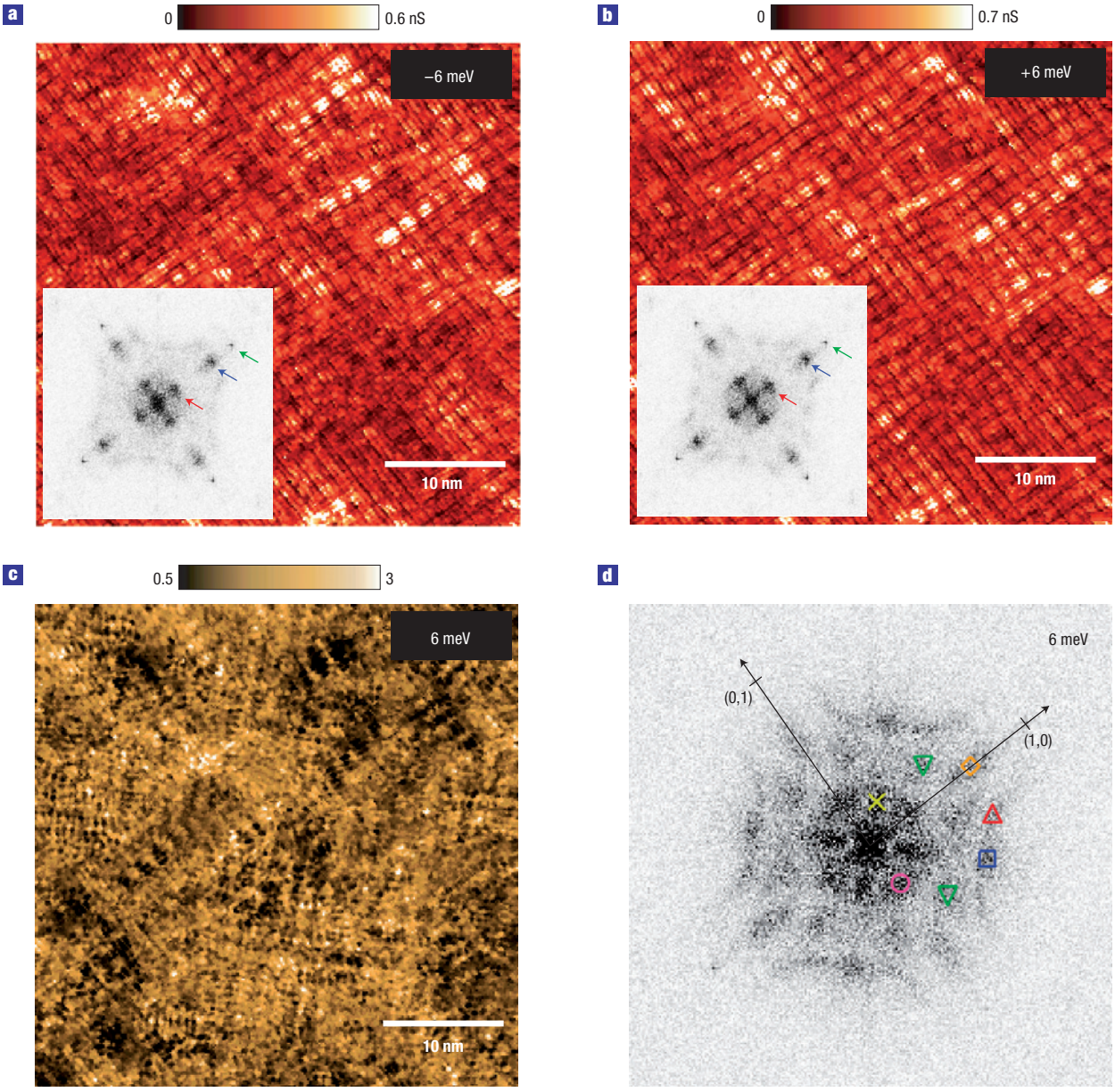

Figure 3 Fourier-transform STS results on Na-CCOC ($T_c \sim 28$ K, $x \sim 0.14$) demonstrating the QPI in the conductance-ratio map $Z(\mathbf{r}, E) \equiv g(\mathbf{r}, +E)/g(\mathbf{r}, -E)$. **a**, The filled-state $g(\mathbf{r}, E)$ taken at -6 meV. (Set-up conditions: $V_s = +150$ mV and $I_t = 100$ pA.) This map is basically dominated by the apparent CB g modulation, which consists of components with wavelengths of $4a_0$, $4a_0/3$ and a_0 (ref. 9) as manifested by $|g(\mathbf{q}, E)|$ shown in the inset. (Red, dark blue and green arrows denote $4a_0$, $4a_0/3$ and a_0 components, respectively.) The same features are also seen in $g(\mathbf{r}, E)$ and $|g(\mathbf{q}, E)|$ in the empty state ($E = +6$ meV) as shown in **b**. Note that $g(\mathbf{r}, E)$ (and $|g(\mathbf{q}, E)|$) are very similar between filled and empty states and local conductance maxima/minima occur predominantly at the same location. **c**, The conductance-ratio map $Z(\mathbf{r}, E)$ calculated from **a** and **b**. The CB g modulation almost completely disappears and a new type of modulation emerges. **d**, $|Z(\mathbf{q}, E)|$ obtained by Fourier transformation of $Z(\mathbf{r}, E)$. The **q** vectors which characterize $Z(\mathbf{r}, E)$ are clearly represented by local maxima (dark spots) in the image. All of the **q** vectors expected from the octet model of QPI are observed in $|Z(\mathbf{q}, E)|$, as indicated by symbols that correspond to those in Fig. 1c. Note that no extra **q** vector is detected. This result strongly indicates that the modulation in $Z(\mathbf{r}, E)$ originates from the QPI.

to the heavily underdoped samples are also seen in $g(\mathbf{r}, E)$ and an averaged tunnelling spectrum; $g(\mathbf{r}, E)$ shows apparent CB modulations (Fig. 2b) whereas the averaged spectrum shows a V-shaped pseudogap below ~100 meV (Fig. 2c).

We next focus on spectroscopic features at low energies. As shown in Fig. 2d, inside the V-shaped pseudogap, we found a pair of kinklike features at about ±10 meV. Thus, there are at least two energy scales in the system: the ~100 meV pseudogap and the ~10 meV kink. It was found that the low-energy region below the two kinklike features tends to be filled up homogeneously over the field of view under magnetic fields (up to 11 T) or at elevated temperatures (up to 20 K), suggesting that superconductivity plays a role for the suppression of low-energy QP states. These observations motivated us to search for QPI to directly probe the SG dispersion in this low-T_c but nearly optimally doped high-T_c cuprate.

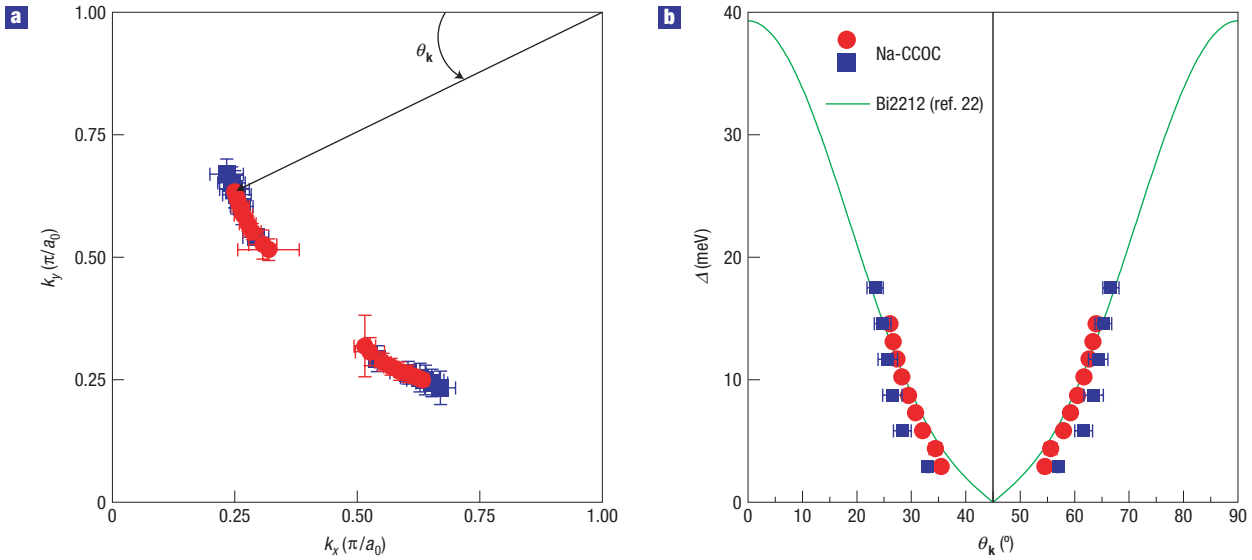

Figure 4 The obtained FS and the SG dispersion for Na-CCOC ($T_c \sim 28$ K, $x \sim 0.14$). a, The locus of octet ends of banana-shaped CCEs in a quadrant of the first Brillouin zone, which represents the underlying FS. The data are symmetrized about the diagonal owing to mirror symmetry. The results for two different samples are plotted in red circles and blue squares, respectively. In the analysis, we used four independent $\mathbf{q}_4(E) = (\pm 2k_x(E), 2k_y(E)), (2k_y(E), \pm 2k_x(E))$, which were clearly observed between 3 meV $< E <$ 15 meV. The other $\mathbf{q}_i$ vectors gave us consistent results but the observed energy range was narrower. The error bars represent the statistical scatters. **b**, The SG plotted as a function of the FS angle θ_k defined in **a**. The two different symbols have the same meaning as in **a**. The green line represents the SG dispersion for nearly optimally doped Bi2212 with $T_c \sim 86$ K (ref. 22). Even though T_c values differ by a factor of three between these two compounds, the SG dispersions are very similar.

QPI patterns in Bi2212 have been observed in raw $g(\mathbf{r}, E)$ or $|g(\mathbf{q}, E)|$ (refs 10,21,22). However, in the case of Na-CCOC ($T_c \sim 28$ K, $x \sim 0.14$), $g(\mathbf{r}, E)$ and $|g(\mathbf{q}, E)|$ are primarily governed by the apparent CB g modulations as shown in Fig. 3a,b and a clear signature of QPI is difficult to recognize. Thus, we need to find a new technique to extract QPI patterns which may be hidden behind the apparent CB g modulations.

SEPARATION OF QPI FROM THE 'CHECKERBOARD'

To separate QPI from the apparent CB g modulations we consider the spatial-phase relations in the g modulations. A comparison between the positive and negative bias $g(\mathbf{r}, \pm E)$ shows that CB modulations in $g(\mathbf{r}, +E)$ and $g(\mathbf{r}, -E)$ are spatially quite similar and the local conductance maxima/minima occur predominantly at the same location as shown in Fig. 3a,b. In other words, the apparent CB g modulations have the same wavelength and are in phase across the Fermi energy. The QPI patterns should also have the same wavelength in $g(\mathbf{r}, +E)$ and $g(\mathbf{r}, -E)$ because $E(\mathbf{k})$ is expected to be particle–hole symmetric as shown in Fig. 1a. The spatial-phase relation for QPI is not known precisely but it is plausible that there is a phase difference between $g(\mathbf{r}, +E)$ and $g(\mathbf{r}, -E)$ as there is a sum-rule $\sum_n v_n^2(\mathbf{r}) + u_n^2(\mathbf{r}) = 1$ between particle-like and holelike amplitudes of the Bogoliubov quasiparticle, $v_n^2(\mathbf{r})$ and $u_n^2(\mathbf{r})$, where n is an appropriate quantum number[38]. Therefore, the QPI pattern may be extracted by means of the spatial-phase-sensitive method if they have a non-trivial phase difference.

For this purpose, we propose to examine the ratio map defined by $Z(\mathbf{r}, E) \equiv g(\mathbf{r}, +E)/g(\mathbf{r}, -E)$ and its Fourier transform $|Z(\mathbf{q}, E)|$. Let us introduce a basic property of $|Z(\mathbf{q}, E)|$. If the conductance modulation amplitude at finite $\mathbf{q}$, $g_q^{\pm} \equiv g(\mathbf{q}, \pm E)$, is much smaller than the uniform component $g_0^{\pm} \equiv g(\mathbf{q} = 0, \pm E)$, $|Z(\mathbf{q}, E)|$ can be approximated as (to the first order) $|Z(\mathbf{q}, E)| \approx (g_0^+/g_0^-)|(g_q^+/g_0^+) - (g_q^-/g_0^-)|$. In the present case, the relation $|g_q^{\pm}|/g_0^{\pm} \ll 1$ holds for all the energies studied. Therefore, the above approximation is well justified. Note that $|Z(\mathbf{q}, E)|$ is sensitive to the relative signs between $g(\mathbf{q}, +E)$ and $g(\mathbf{q}, -E)$. (Note that $g_0^{\pm} > 0$.) Namely, taking the ratio reduces the in-phase component.

In Fig. 3c and d, respectively, we show the measured $Z(\mathbf{r}, E = 6\,\text{meV})$ and the Fourier transform $|Z(\mathbf{q}, E = 6\,\text{meV})|$. It is immediately evident that the CB g modulation, which dominates $g(\mathbf{r}, E)$ and $|g(\mathbf{q}, E)|$, almost completely disappears. Moreover, most satisfyingly, another type of modulation emerges. The features of the new modulations are clearly manifested in $|Z(\mathbf{q}, E)|$, where numerous spots are observed at incommensurate $\mathbf{q}$ vectors. All of these $\mathbf{q}$ vectors are consistently explained in terms of the octet model[22] of QPI as shown by symbols in Fig. 3d. Thus the existence of the QPI effect and therefore the coherent Bogoliubov quasiparticle of the d-wave superconducting state are clearly confirmed for the first time in Na-CCOC. The origin of the enhanced QPI pattern and detailed intensity distribution in $|Z(\mathbf{q}, E)|$ are interesting subjects for future theoretical research.

We would like to note that the ratio Z has another important feature besides its phase sensitivity[39]. In general, tunnelling conductance $g(\mathbf{r}, E = eV)$ is given by

$$g(\mathbf{r}, eV) = \frac{eI_t N(\mathbf{r}, eV)}{\int_0^{eV_s} N(\mathbf{r}, E)\mathrm{d}E}.$$

Here, e is a unit charge, I_t and V_s are the set-up current and bias voltage for feedback, respectively, and N is a local DOS. Note that g is not proportional to N but is normalized by the integrated N, which is strongly influenced by the set-up conditions through V_s. On the other hand, $Z(\mathbf{r}, eV)$ reflects the ratio of the N precisely, because the denominator and prefactor eI_t are exactly cancelled out by taking the ratio[39]. This fact means that observed QPI is an intrinsic phenomenon free from any set-point-related issues, which inevitably contaminate $g(\mathbf{r}, E)$ and $|g(\mathbf{q}, E)|$. In contrast, there is a

possibility that CB g modulation is affected by the set-point effect, because it disappears in Z at least below the kink energy where QPI is observed. Therefore, it is important to search for the possible electronic superstructure using the set-point-effect-free method.

Recently, ratio analyses at high energy ($\sim$150 meV) in underdoped Na-CCOC and Bi2212 have revealed the existence of an electronic-cluster-glass (ECG) state characterized by the four-Cu–Cu-distance-wide bond-centred unidirectional electronic domains dispersed throughout without long-range order[39]. Similarities between ECG and CB g modulation (for example, characteristic length scale of four Cu–Cu distances) imply close relations between the two. It is interesting to note that apparently different phenomena, high-energy ECG and low-energy QPI, have been detected in similar analysis schemes depending on the energy scale. Given the fact that the ratio analysis extracts intrinsic information on the electronic states, establishing the relation between ECG and QPI, which may represent localized and delocalized electronic states, respectively, represents a key goal for this field.

INSIGHTS FROM THE QPI ANALYSIS

To analyse the observed Na-CCOC QPI quantitatively, we measured $\mathbf{q}_i$ at different E and determined the energy-dependent locations of the octet ends of 'bananas' in $\mathbf{k}$ space. The obtained locus $\mathbf{k}(E) = (k_x(E), k_y(E))$ can be interpreted as a normal-state FS. We plot the obtained loci for two different samples in Fig. 4a. The result is consistent with a cylindrical FS centred around (π, π), which is inferred from ARPES on underdoped samples[12].

We can determine the SG dispersion $\Delta(\mathbf{k})$ from $\mathbf{k}(E)$ as well[22]. In Fig. 4b, we plot the measured gap energy as a function of FS angle $\theta_{\mathbf{k}}$ about (π, π). For comparison, SG dispersion of optimally doped Bi2212 (ref. 22) is shown by a green line. Apparently, SG dispersions of these two compounds are quite similar. Because T_c values are very different between Na-CCOC ($T_c \sim 28$ K) and Bi2212 ($T_c \sim 86$ K), we can conclude that the SG dispersion in the nodal region does not set the energy scale which determines T_c alone.

It is worthwhile to note that QPI in optimally doped Na-CCOC is observed in a rather limited part of the FS near the node ($25° < \theta_{\mathbf{k}} < 65°$). This suggests that available quasiparticle states are missing from the antinodal region[40–42] or that the antinodal quasiparticles may not have a correlation length long enough to produce interference due to disorder[43]. In accord with this, well-defined coherence peaks that manifest the coherent quasiparticle states in the antinodal region[10,22] are not observed in the tunnelling spectra, as shown in Fig. 2c and d. In the ARPES data on the $x \sim 0.12$ ($T_c \sim 22$ K) sample, with slightly lower hole concentration than the present samples, the spectral weight in the antinodal region is still substantially suppressed, which was pointed out to be linked with CB g modulations[12]. Here we postulate that such incoherent antinodal states are not responsible for forming phase-coherent Cooper pairs. If this picture is correct, superconductivity is supported only by the coherent part of the FS around the node, namely, a d-wave SG opens on the so-called Fermi arc. This conjecture predicts that the energy scale which sets T_c is determined not only by the SG dispersion around the node but also by the effective 'arc length'. Analogous proposals have also been made on the basis of the doping dependence of the gap amplitude[44].

Finally, we compare the tunnelling spectrum of Na-CCOC with that of Bi2212. In optimally doped Bi2212, well-defined coherence peaks are ubiquitous[10] and thus the entire FS may be responsible for superconductivity. On the other hand, in underdoped Bi2212, a different type of spectrum characterized by the V-shaped gap without a clear coherence peak appears, while the QPI signal is still there[10]. This spectrum is very similar to the spectrum of Na-CCOC (refs 6,9). Interestingly, in underdoped Bi2212, a non-dispersive CB g modulation is also seen in the region where this type of spectrum is observed[10]. Therefore, it is reasonable to infer that the V-shaped gap without a clear coherence peak, the destruction of the antinodal state and the CB g modulation go hand in hand and are universal in high-T_c cuprates. Another important common feature observed in both Na-CCOC and Bi2212 is that this state is superconducting, with long-lived Bogoliubov quasiparticles, which are manifested by QPI.

CONCLUSION

We report the first observation of QPI associated with d-wave superconductivity in Na-CCOC. This provides us with firm evidence for the coexistence of d-wave superconductivity and CB g modulation, presumably associated with the ECG state, which probably represents the nodal/antinodal dichotomy in $\mathbf{k}$ space. The striking similarity of SG dispersions between Na-CCOC ($T_c \sim 28$ K) and Bi2212 ($T_c \sim 86$ K) in the nodal regions strongly suggests that the nodal/antinodal dichotomy is controlling T_c from material to material. Further exploration of $\mathbf{k}$-space physics, we believe, should help identify a key ingredient to enhance T_c of cuprate superconductors. A novel analysis, g-ratio or Z analysis, was developed to separate QPI signals from the CB g modulation. It is quite sensitive to the spatial-phase difference in quantum admixtures of particle-like and holelike states and will be a powerful probe to explore the quasiparticle interferences in superconductors and possibly other quantum condensates.

METHODS

Na-CCOC single crystals were grown by the flux method under high pressure of the order of several gigapascals[37]. By optimizing the synthesis conditions, we succeeded in growing suitably sized nearly optimally doped single crystals with $T_c \sim 25$ K and 28 K, which correspond to $x \sim 0.13$ and 0.14, respectively.

SI-STM measurements were carried out with a newly developed ultrahigh-vacuum very-low-temperature scanning tunnelling microscope at RIKEN[45]. Samples were cleaved *in situ* at 77 K under ultrahigh vacuum and were immediately transferred to the STM unit, which was kept at low temperature (<10 K). Tungsten scanning tips were sharpened and characterized *in situ* with atomic resolution by a field-ion microscope, which is built in to the STM chamber. All the data were taken at a temperature $T \sim 0.4$ K.

Received 14 February 2007; accepted 19 September 2007; published 28 October 2007.

References

1. Fischer, Ø., Kugler, M., Maggio-Aprile, I., Berthod, C. & Renner, C. Scanning tunneling spectroscopy of high-temperature superconductors. *Rev. Mod. Phys.* **79**, 353–419 (2007).
2. Cren, T., Roditchev, D., Sacks, W. & Klein, J. Nanometer scale mapping of the density of states in an inhomogeneous superconductor. *Eur. Phys. Lett.* **54**, 84–90 (2001).
3. Howald, C., Fournier, P. & Kapitulnik, A. Inherent inhomogeneities in tunneling spectra of $Bi_2Sr_2CaCu_2O_{8-x}$ crystals in the superconducting state. *Phys. Rev. B* **64**, 100504 (2001).
4. Pan, S. H. *et al.* Microscopic electronic inhomogeneity in the high-T_c superconductor $Bi_2Sr_2CaCu_2O_{8+x}$. *Nature* **413**, 282–285 (2001).
5. Lang, K. M. *et al.* Imaging the granular structure of high-T_c superconductivity in underdoped $Bi_2Sr_2CaCu_2O_{8+\delta}$. *Nature* **415**, 412–416 (2002).
6. Kohsaka, Y. *et al.* Imaging nano-scale electronic inhomogeneity in lightly doped Mott insulator $Ca_{2-x}Na_xCuO_2Cl_2$. *Phys. Rev. Lett.* **93**, 097004 (2004).
7. Hoffman, J. E. *et al.* A four unit cell periodic pattern of quasi-particle states surrounding vortex cores in $Bi_2Sr_2CaCu_2O_{8+\delta}$. *Science* **295**, 466–469 (2002).
8. Vershinin, M. *et al.* Local ordering in the pseudogap state of the high-T_c superconductor $Bi_2Sr_2CaCu_2O_{8+\delta}$. *Science* **303**, 1995–1998 (2004).
9. Hanaguri, T. *et al.* A 'checkerboard' electronic crystal state in lightly hole-doped $Ca_{2-x}Na_xCuO_2Cl_2$. *Nature* **430**, 1001–1005 (2004).
10. McElroy, K. *et al.* Coincidence of checkerboard charge order and antinodal state decoherence in strongly underdoped superconducting $Bi_2Sr_2CaCu_2O_{8+\delta}$. *Phys. Rev. Lett.* **94**, 197005 (2005).
11. Damascelli, A., Hussain, Z. & Shen, Z.-X. Angle-resolved photoemission studies of the cuprate superconductors. *Rev. Mod. Phys.* **75**, 473–541 (2003).
12. Shen, K. M. *et al.* Nodal quasiparticles and antinodal charge ordering in $Ca_{2-x}Na_xCuO_2Cl_2$. *Science* **307**, 901–904 (2005).
13. Yoshida, T. *et al.* Low-energy electronic structure of the high-T_c cuprates $La_{2-x}Sr_xCuO_4$ studied by angle-resolved photoemission spectroscopy. *J. Phys. Condens. Matter* **19**, 125209 (2007).
14. Tanaka, K. *et al.* Distinct Fermi-momentum-dependent energy gaps in deeply underdoped Bi2212. *Science* **314**, 1910–1913 (2006).

15. Norman, M. R. *et al.* Destruction of the Fermi surface in underdoped high-T_c superconductors. *Nature* **392**, 157–160 (1998).
16. Tsuei, C. C. & Kirtley, J. R. Pairing symmetry in cuprate superconductors. *Rev. Mod. Phys.* **72**, 969–1016 (2000).
17. Le Tacon, M. *et al.* Two energy scales and two distinct quasiparticle dynamics in the superconducting state of underdoped cuprates. *Nature Phys.* **2**, 537–543 (2006).
18. Gomes, K. K. *et al.* Visualizing pair formation on the atomic scale in the high-T_c superconductor $Bi_2Sr_2CaCu_2O_{8+\delta}$. *Nature* **447**, 569–572 (2007).
19. Boyer, M. C. *et al.* Imaging the two gaps of the high-T_c superconductor Pb-$Bi_2Sr_2CuO_{6+x}$. *Nature Phys.* published online 16 September 2007 (doi:10.1038/nphys725).
20. Timusk, T. & Statt, B. The pseudogap in high-temperature superconductors: an experimental survey. *Rep. Prog. Phys.* **62**, 61–122 (1999).
21. Hoffman, J. E. *et al.* Imaging quasiparticle interference in $Bi_2Sr_2CaCu_2O_{8+\delta}$. *Science* **297**, 1148–1151 (2002).
22. McElroy, K. *et al.* Relating atomic-scale electronic phenomena to wave-like quasiparticle states in superconducting $Bi_2Sr_2CaCu_2O_{8+\delta}$. *Nature* **422**, 592–596 (2003).
23. Wang, Q. & Lee, D.-H. Quasiparticle scattering interference in high temperature superconductors. *Phys. Rev. B* **67**, 020511 (2003).
24. Zhang, D. & Ting, C. S. Energy-dependent modulations in the local density of states of the cuprate superconductors. *Phys. Rev. B* **67**, 100506 (2003).
25. Pereg-Barnea, T. & Franz, M. Theory of quasiparticle interference patterns in the pseudogap phase of the cuprate superconductors. *Phys. Rev. B* **68**, 180506 (R) (2003).
26. Capriotti, L., Scalapino, D. J. & Sedgewick, R. D. Wave-vector power spectrum of the local tunneling density of states: Ripples in a *d*-wave sea. *Phys. Rev. B* **68**, 014508 (2003).
27. Zhu, L., Atkinson, W. A. & Hirschfeld, P. J. Power spectrum of many impurities in a *d*-wave superconductor. *Phys. Rev. B* **69**, 060503(R) (2004).
28. Pereg-Barnea, T. & Franz, M. Quasiparticle interference patterns as a test for the nature of the pseudogap phase in the cuprate superconductors. *Int. J. Mod. Phys. B* **19**, 731–761 (2005).
29. Dell'Anna, L., Lorenzana, J., Capone, M., Castellani, C. & Grilli, M. Effect of mesoscopic inhomogeneities on local tunneling density of states in cuprates. *Phys. Rev. B* **71**, 064518 (2005).
30. Cheng, M. & Su, W. P. Local density of states and angle-resolved photoemission spectral function of an inhomogeneous *d*-wave superconductor. *Phys. Rev. B* **72**, 094512 (2005).
31. Nunner, T. S. *et al.* Fourier transform spectroscopy of *d*-wave quasiparticles in the presence of atomic scale pairing disorder. *Phys. Rev. B* **73**, 104511 (2006).
32. Hasegawa, Y. & Avouris, Ph. Direct observation of standing wave formation at surface steps using scanning tunneling spectroscopy. *Phys. Rev. Lett.* **71**, 1071–1074 (1993).
33. Crommie, M. F., Lutz, C. P. & Eigler, D. M. Imaging standing waves in a two-dimensional electron gas. *Nature* **363**, 524–527 (1993).
34. Sprunger, P. T., Petersen, L., Plummer, E. W., Lægsgaard, E. & Besenbacher, F. Giant Friedel oscillations on the beryllium(0001) surface. *Science* **275**, 1764–1767 (1997).
35. Tinkham, M. *Introduction to Superconductivity* 2nd edn, 43 (McGraw Hill, New York, 1996).
36. Hiroi, Z., Kobayashi, N. & Takano, M. Probable hole-doped superconductivity without apical oxygens in $(Ca,Na)_2CuO_2Cl_2$. *Nature* **371**, 139–141 (1994).
37. Kohsaka, Y. *et al.* Growth of Na-doped $Ca_2CuO_2Cl_2$ single crystals under high pressures of several GPa. *J. Am. Chem. Soc.* **124**, 12275–12278 (2002).
38. Balatsky, A. V., Vekhter, I. & Zhu, J.-X. Impurity-induced states in conventional and unconventional superconductors. *Rev. Mod. Phys.* **78**, 373–433 (2006).
39. Kohsaka, Y. *et al.* An intrinsic bond-centered electronic glass with unidirectional domains in underdoped cuprates. *Science* **314**, 1380–1385 (2007).
40. Furukawa, N., Rice, T. M. & Salmhofer, M. Truncation of a two-dimensional FS due to quasiparticle gap formation at the saddle points. *Phys. Rev. Lett.* **81**, 3195–3198 (1998).
41. Wen, X.-G. & Lee, P. A. Theory of quasiparticles in the underdoped high-T_c superconducting state. *Phys. Rev. Lett.* **80**, 2193–2196 (1998).
42. Li, J.-X., Wu, C.-Q. & Lee, D.-H. Checkerboard charge density wave and pseudogap of high-T_c cuprates. *Phys. Rev. B* **74**, 184515 (2006).
43. Garg, A., Randeria, M. & Trivedi, N. Strong correlations lead to protected low energy excitations in disordered *d*-wave superconductors. Preprint at <http://arXiv.org/cond-mat/0609666> (2006).
44. Oda, M., Dipasupil, R. M., Momono, N. & Ido, M. Hyperbolic dependence of $2\Delta_0$ vs. T_c ratio on hole-doping level in high-T_c cuprates: Energy scale in determining T_c. *J. Phys. Soc. Jpn.* **69**, 983–984 (2000).
45. Hanaguri, T. Development of high-field STM and its application to the study on magnetically-tuned criticality in $Sr_3Ru_2O_7$. *J. Phys. Conf. Ser.* **51**, 514–521 (2006).

Acknowledgements

The authors thank A.V. Balatsky, C.-M. Ho, D.-H. Lee, K. Machida, A. Mackenzie, K. McElroy, T. Tohyama, J. Zaanen and F.-C. Zhang for discussions. They also thank J. Matsuno and P. Sharma for critical readings. T.H., M.T. and H.T. are supported by a Grant-in-Aid for Scientific Research from the Ministry of Education, Culture, Sports, Science and Technology of Japan. J.C.D. and Y.K. acknowledge support from Brookhaven National Laboratory under contract No DE-AC02-98CH1886 with the US Department of Energy, from the US Department of Energy Award No DE-FG02-06ER46306 and from the US Office of Naval Research.
Correspondence and requests for materials should be addressed to T.H.

Author contributions

T.H. was responsible for all aspects of this project except sample growth. Y.K., J.C.D. and C.L. contributed the project planning and data analysis. I.Y., M.A., M.T. and K.O. grew samples and M.O. contributed the STM measurements. H.T. contributed the project planning and managed the whole project.